Coherence-controlled holographic microscopy in diffuse media

Martin Lošťák,[1,2,*] **Radim Chmelík,**[1,2] **Michala Slabá,**[1,2] **and Tomáš Slabý** [1]

[1] *Institute of Physical Engineering, Faculty of Mechanical Engineering, Brno University of Technology, Technická 2, 616 69 Brno, Czech Republic*

[2] *CEITEC - Central European Institute of Technology, Brno University of Technology, Technická 10, 616 00 Brno, Czech Republic*

[*] *martin.lostak@email.cz*

Abstract: Low-coherence interferometric microscopy (LCIM) enables to image through scattering media by filtration of ballistic light from diffuse light. The filtration mechanism is called coherence gating. We show that coherence-controlled holographic microscope (CCHM), which belongs to LCIM, enables to image through scattering media not only with ballistic light but also with diffuse light. The theoretical model was created which derives the point spread function of CCHM for imaging through diffuse media both with ballistic and diffuse light. The results of the theoretical model were compared to the experimental results. In the experiment the resolution chart covered by a ground glass was imaged. The experimental results are in the good agreement with the theoretical results. It was shown both by experiments and the theoretical model, that with ballistic and diffuse light we can obtain images with diffraction limited resolution.

OCIS codes: (090.0090) Holography; (110.0113) Imaging through turbid media; (110.4980) Partial coherence in imaging; (120.5050) Phase measurement; (170.1790) Confocal microscopy; (180.3170) Interference microscopy.

References and links

1. M. Minsky, "Memoir on inventing the confocal scanning microscope," Scanning **10**, 128–138 (1988).
2. T. Wilson, *Confocal Microscopy* (Academic Press, 1990).
3. M. Kempe, W. Rudolph, and E. Welsch, "Comparative study of confocal and heterodyne microscopy for imaging through scattering media," J. Opt. Soc. Am. A **13**, 46–52 (1996).
4. M. Kempe, A. Genack, W. Rudolph, and P. Dorn, "Ballistic and diffuse light detection in confocal and heterodyne imaging systems," J. Opt. Soc. Am. A **14**, 216–223 (1997).
5. J. M. Schmitt, A. Knüttel, and M. Yadlowsky, "Confocal microscopy in turbid media," J. Opt. Soc. Am. A **16**(8) 2226–2235 (1994)
6. J. C. Schotland,"Continuous-wave diffusion imaging," J. Opt. Soc. Am. A **14**(1) 275-279 (1997).
7. N. L. Patel,"Relative capacities of time-gated versus continuous-wave imaging to localize tissue embedded vessels with increasing depth," J. Biomed. Opt. **15**(1) 016015 (2010).
8. B. J. Tromberg, L. O. Svaasand, T. T. Tsay, and R. C.Haskell, "Properties of photon density waves in multiple-scattering media," Appl. Opt. **32** 607–616 (1993).
9. V. Tuchin, *Tissue Optics: Light Scattering Methods and Instruments for Medical Diagnosis* (SPIE Press, 2007).
10. W. Rudolph and M. Kempe, "Trends in optical biomedical imaging," J. Mod. Opt. **44** 1617-1642 (1997).
11. E. Leith and J. Upatnieks, "Reconstructed wavefronts and communication theory," J. Opt. Soc. Am. **52** 1123-1128 (1962).
12. H. Kogelnik, "Holographic image projection through inhomogeneous media," Bell Syst. Tech. J. **44**, 2451–2455 (1965).

#193887 - $15.00 USD Received 29 Aug 2013; revised 11 Nov 2013; accepted 17 Dec 2013; published 18 Feb 2014

13. G. Indebetouw and P. Klysubun, "Imaging through scattering media with depth resolution by use of low-coherence gating in spatiotemporal digital holography," Opt. Lett. **25**, 212–214 (2000).
14. E. Leith, C. Chen, H. Chen, Y. Chen, D. Dilworth, J. Lopez, J. Rudd, P. Sun, J. Valdmanis, and G. Vossler, "Imaging through scattering media with holography," J. Opt. Soc. Am. A **9**, 1148–1153 (1992).
15. S. Tamano, Y. Hayasaki, and N. Nishida, "Phase-shifting digital holography with a low-coherence light source for reconstruction of a digital relief object hidden behind a light-scattering medium," Appl. Opt. **45**, 953–959 (2006).
16. E. Leith and C. Kuei,"Interferometric method for imaging through inhomogeneities," Opt. Lett. **12**, 149–151 (1987).
17. P. Kolman and R. Chmelík,"Coherence-controlled holographic microscope," Opt. Express **18**, 21990-22003 (2010).
18. F. Dubois, C. Yourassowsky, O. Monnom, J. Legros, O Debeir, P. Van Ham, R. Kiss, and C. Decaestecker,"Digital holographic microscopy for the three-dimensional dynamic analysis of in vitro cancer cell migration," J. Biomed. Opt. **11**, 054032 (2006).
19. D. Huang, E. Swanson, C. Lin, J. Schuman, W. Stinson, W. Chang, M. Hee, T. Flotte, K. Gregory, C. Puliafito, et al., "Optical coherence tomography," Science **254**, 1178–1181 (1991).
20. J. Izatt, M. Hee, G. Owen, E. Swanson, and J. Fujimoto, "Optical coherence microscopy in scattering media," Opt. Lett. **19**, 590–592 (1994).
21. E. Leith, "Broad-source image plane holography as a confocal imaging process," Appl. Opt. **33**, 597–602 (1994).
22. Y. Cotte, M. F. Toy, N. Pavillon, and C. Depeursinge, "Microscopy image resolution improvement by deconvolution of complex fields.," Opt. Express **18**, 19462–19478 (2010).
23. Y. Cotte, F. Toy, P. Jourdain, N. Pavillon, D. Boss, P. Magistretti,P. Marquet, and C. Depeursinge, "Marker-free phase nanoscopy," Nature Photon. **7**, 113–117 (2013).
24. M. Mir,S. D. Babacan, M. Bednarz, M. N. Do, I. Golding, G. Popescu, "Visualizing Escherichia coli sub-cellular structure using sparse deconvolution spatial light interference tomography," PLOS ONE **7**, e39816 (2012).
25. M. Lošťák, P. Kolman, Z. Dostál, and R. Chmelík, "Diffuse light imaging with a coherence controlled holographic microscope," Proc. SPIE **7746**, 77461N (2010).
26. T. Slabý, M. Antoš, Z. Dostál, P. Kolman, and R. Chmelík, "Coherence-controlled holographic microscope," Proc. SPIE **7746**, 77461R (2010).
27. T. Slabý, P. Kolman, Z. Dostál, M. Antoš, M. Lošťák, and R. Chmelík, "Off-axis setup taking full advantage of incoherent illumination in coherence-controlled holographic microscope," Opt. Express **21**, 14747–14762 (2013).
28. R. Chmelík, "Three-dimensional scalar imaging in high-aperture low-coherence interference and holographic microscopes," J. Mod. Opt. **53**, 2673–2689 (2006).
29. E. N. Leith and B. J. Chang, "Space-invariant holography with quasi-coherent light," Appl. Opt. **12**, 1957—1963 (1973).
30. M. Born and E. Wolf, *Principles of Optics*, 7th expanded ed. (Cambridge University, 2002).
31. J. Goodman, *Introduction to Fourier Optics*, 2nd ed. (McGraw-Hill, 1996)
32. W. H. Press, *Numerical Recipes: The Art of Scientific Computing*, 3rd ed. (Cambridge University, 2007).
33. C. N. Kurtz, "Transmittance characteristics of surface diffusers and the design of nearly band-limited binary diffusers," J. Opt. Soc. Am. **62**, 982–989 (1972).
34. R. B. Crane, "Use of a laser-produced speckle pattern to determine surface roughness," J. Opt. Soc. Am. **60**, 1658–1663 (1970).

1. Introduction

When imaging through turbid media, such as cell structures, the image is degraded by the light scattered out of the object plane. The aim of some light microscopy techniques is to exclude this multiply scattered (diffuse) light from forming the image. In order to do that confocal microscopy [1–5] can be used. The other possibility, how to filter the scattered light is to use the different properties of ballistic and diffuse light.

In biology, there are many techniques which do not aim to eliminate diffuse light, but on the contrary they can use diffuse light for obtaining the information from specimen. For example, the so called continuous-wave imaging [6, 7], techniques that use diffuse photon density waves [8] etc. However, these techniques have very often much lower resolution than classic light microscopy.

Optical medical imaging techniques usually use diffuse light for imaging and they are summarized in few comprehensive publications [9,10]. The resolving power of these techniques us-

#193887 - $15.00 USD Received 29 Aug 2013; revised 11 Nov 2013; accepted 17 Dec 2013; published 18 Feb 2014

ing diffuse-light is much worse than in the case of ballistic-light techniques. Diffuse-light techniques, however, have their main advantage consisting in the fact that they can image through much thicker and denser media. The resolution and also the maximum thickness of studied objects are in the range of millimeters to centimeters depending on the particular technique used. In contrast to it the ballistic techniques have the diffraction limited resolution.

Besides confocal microscopy the interference techniques are used for imaging through diffuse media using filtering of ballistic light from diffuse light. These interference techniques, with the exception as for example phase conjugation technique [11, 12], usually use low-coherence light source. Therefore they can be called low-coherence interferometry (LCI) techniques. The mechanism responsible for filtering ballistic light from diffuse light in LCI is called coherence gating [3, 13, 14]. It means that diffuse light from the object arm interacts with light from the reference arm outside coherence volume. Therefore the two beams cannot interfere.

The ability of LCI to image through various diffuse media has been demonstrated in many publications already [3], [13–21]. Typical diffuse media used in optical publications are for example the solution of milk in water [15], latex spheres in water [4]. However the most often used dry diffuse medium is ground glass [13, 16, 17]. All different types of biological material can be used as a diffuse medium, for example a collagen gel [18] or a soft tissue [14]. The historical overview of holographic techniques using low-coherence sources for imaging through diffuse media is a part of publication [14]. A very specific group of LCI is optical coherence tomography (OCT) [19] and optical coherence microscopy (OCM) [20]. Their main significance lies in the fact that they can be used in-vivo and especially OCT is nowadays a common technique used in ophthalmology.

Although the experimental results of imaging through diffuse media with LCI are currently part of many publications, the quantitative description of the overall imaging process is quite rare yet. Only few publications are the exceptions. In [14] and [21], the influence of diffuse medium on the point spread function (PSF) of LCI microscope is discussed. It is shown here schematically how PSF is altered by a diffuse medium, but there is no quantitative expression for PSF. In [3] and [15], PSF is determined experimentally by imaging a resolution test chart. In both [3] and [15], it is concluded that resolving power of LCI is reduced when imaging through diffuse media. The main reason for that is very poor level of signal to noise ratio (SNR). Therefore averaging of more images was utilized which improved resolution to the diffraction limit. Again no computation of PSF was provided. Recently, there appeared few papers which deal with computations of PSF in digital holography [22–24]. Authors here are using the PSF computations for deconvolution in order to improve the resolving power. Anyway, nowhere to our knowledge, there has appeared any publication so far describing a possibility of imaging by diffuse light in an LCI microscope.

In the present publication, which links to our previous work [25] we show that in an off-axis LCI microscope which we call coherence-controlled holographic microscope (CCHM), we are able to image through diffuse media both with ballistic and diffuse light. This statement is supported both by the theoretical model of PSF and by the experimental results which prove the theory. As a result of both the theoretical and the experimental parts we show here that by imaging in CCHM we are able to image with both ballistic and diffuse light preserving the diffraction limited resolution. The largest limitation is mainly low SNR, therefore this type of imaging is possible only for certain level of the diffuser strength.

As the aim of the article is to explain the imaging principle clearly, the model of a diffuser in this paper is limited to thin (one layer) diffuser only.

#193887 - $15.00 USD Received 29 Aug 2013; revised 11 Nov 2013; accepted 17 Dec 2013; published 18 Feb 2014

2. Theory

2.1. *Optical setup of CCHM*

The principle of CCHM (Fig. 1) is described in detail in [26, 27]. Light coming from an extended and polychromatic source S is split by the beam splitter BS_1 into two arms, the object and the reference arm. Both arms are put together again in the output plane OP where the detector D is placed. The optical path difference between the reference and the object arm, measured from beam splitter to the output plane OP is lower than the coherence length.

In the object arm, a light beam goes through a specimen and the beam comes to the output plane in the direction of its normal line. In the reference arm, the beam goes through a reference object and the beam is diffracted on the diffraction grating DG in such a way that the reference beam enters the output plane OP at an angle β, while angle β depends on the beam wavelength. The output plane OP is optically conjugated with the plane of the diffraction grating DG and simultaneously with the object planes Sp and R of the objective lenses O_1 and O_2, respectively.

Due to off-axis arrangement of the microscope an image-plane hologram with a spatial carrier frequency f_c is formed on the detector D. This fact enables one to reconstruct the complex amplitude of object wave just from a single hologram [17, 28]. Moreover, holograms created in CCHM are achromatic and spatially invariant [29] thanks to the fact that diffraction grating is placed in a plane conjugated with the object plane.

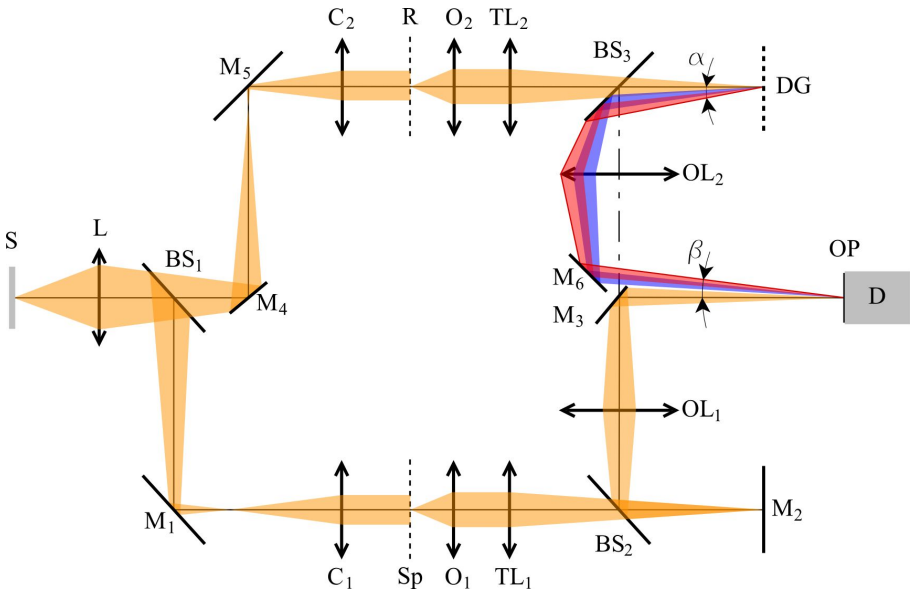

Fig. 1. Optical setup of CCHM. Incoherent light source (S), relay lens (L), beam splitters (BS), mirrors (M), condensers (C), object plane (Sp), reference plane (R), microscope objectives (O), tube lenses (TL), diffraction grating (DG), output lens (OL), output plane (OP), detector (D). Figure adapted, with permission, from [27].

2.2. *Principle of imaging in CCHM through diffuse medium*

The principle of imaging in CCHM through diffuse media is explained with the aid of the simplified drawings in Fig. 2. To illustrate the principle more easily the output plane OP is depicted

#193887 - $15.00 USD Received 29 Aug 2013; revised 11 Nov 2013; accepted 17 Dec 2013; published 18 Feb 2014

separately in each arm. It follows from the Van Cittert-Zernike theorem, that if we consider the light in the object plane of the condensers C_1, C_2 (see Fig. 1) to be spatially incoherent, then we can consider the sections IS_1 and IS_2 which are conjugated with the object planes Sp and R, respectively, to be spatially incoherent sources (see [30]).

In the reference arm, any point A of imaginary source IS_2 is imaged in the output plane as point A_R. The light forming this image A_R can interfere only with that light from the object arm, which is emitted from the conjugated point A of imaginary source IS_1, because any point A of IS_1 is mutually coherent only with the corresponding point A in IS_1. This point A is imaged in the object arm as a point A_0, which coincides with A_R.

If the specimen is planar and if it is placed in the object plane Sp, then the coincidence of points A_0 and A_R is valid for all points of the sources IS_1, IS_2 and thus for the whole field of view (Fig. 2(a)). It means, that all the light transmitted or scattered by the specimen contributes to interference, thus forming the signal.

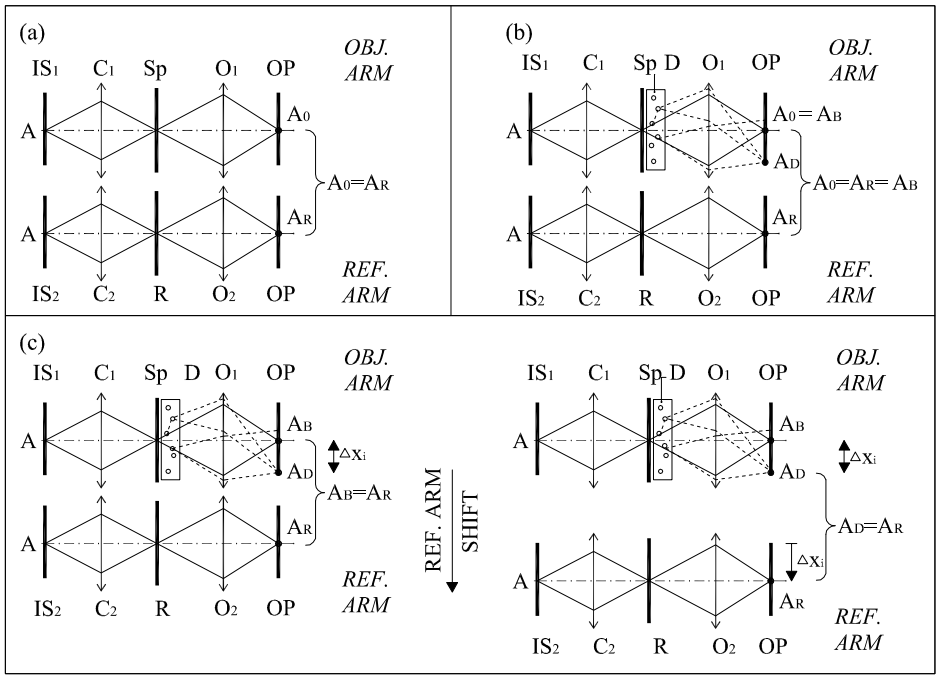

Fig. 2. Simplified drawings for explanation of principle of imaging in CCHM through diffuse medium by ballistic and diffuse light. IS_1, IS_2...imaginary sources in object planes of the condensers C_1, C_2. Sp, R...object planes of microscope objectives O_1, O_2. D...diffuser. A_O, A_R...images of point A in the output plane OP. A_B...ballistic image of point A. A_D...diffuse image of point A. Dotted line...scattered light, continuous line...unscattered light. a) Imaging without diffuser. b) Imaging with diffuser by ballistic light, mutual shift $\Delta x_i = 0$. c) Imaging with diffuser by diffuse light, reference arm is shifted by nonzero Δx_i.

However the situation is changed, if a diffuser is placed behind the specimen. In the reference arm the situation remains unchanged, but in the object arm the light coming from A is scattered by the diffuser across the output plane.

Only a small portion of light goes through diffuser without being scattered. This light is called “ballistic” light and it preserves its original trajectory. The ballistic light creates the

#193887 - $15.00 USD Received 29 Aug 2013; revised 11 Nov 2013; accepted 17 Dec 2013; published 18 Feb 2014

ballistic image A_B which coincides with both A_O and A_R (Fig. 2(b)). The rest of the light passing through the diffuser is called "diffuse light". Because of coherence only the ballistic light in LCI can interfere with the light from the reference arm and thus coherence gating takes place [13, 28].

Diffuse light therefore creates only the unwanted background. But let's assume now, that the reference arm is laterally shifted so much that A_R is shifted by Δx_i in the output plane as shown in the Fig. 2(c). Then only the diffuse light which is emitted from A and scattered by the diffuser into the point A_D which is coincident with A_R can interfere with A_R, thus creating the signal.By this way it is possible to use diffuse light for forming the image in LCI. In contrast to usual diffuse light techniques, which use both ballistic and diffuse light at once, the above described principle uses either ballistic light (when $\Delta x_i = 0$) or diffuse light (when $\Delta x_i \neq 0$). This intuitive explanation shows the importance of the mutual shift Δx_i, which will be used in following computations.

2.3. CCHM signal computation

Let us assume that extended source S is quasi-monochromatic and let $u_o(\mathbf{q_t^i}, \mathbf{K_t})$ and $u_r(\mathbf{q_t^i}, \mathbf{K_t}) \exp(i2\pi f_c x)$ be complex amplitudes of object and reference waves at the point $\mathbf{q_t^i} = (x^i, y^i)$ in the output plane due to emission of an imaginary point source which is a part of extended source S. Then we can write the intensity in $\mathbf{q_t^i}$ as a result of emission of the imaginary point source, as follows

$$\begin{aligned} i(\mathbf{q_t^i}, \mathbf{K_t}) &= |u_o(\mathbf{q_t^i}, \mathbf{K_t}) + u_r(\mathbf{q_t^i}, \mathbf{K_t}) \exp(i2\pi f_c x^i)|^2 = \\ &= |u_o(\mathbf{q_t^i}, \mathbf{K_t})|^2 + |u_r(\mathbf{q_t^i}, \mathbf{K_t})|^2 + u_o(\mathbf{q_t^i}, \mathbf{K_t}) u_r^*(\mathbf{q_t^i}, \mathbf{K_t}) \exp(-i2\pi f_c x^i) + \\ &+ u_o^*(\mathbf{q_t^i}, \mathbf{K_t}) u_r(\mathbf{q_t^i}, \mathbf{K_t}) \exp(i2\pi f_c x^i), \end{aligned} \tag{1}$$

where $2\pi\mathbf{K} = 2\pi(\mathbf{K_t}, K_z)$ is a wave vector. $\mathbf{K_t} = (K_x, K_y)$ and $K = |\mathbf{K}| = 1/\lambda$ is a wavenumber. Term f_c symbolizes a spatial carrier frequency of the hologram in the output plane [27]. Thanks to the use of Köhler illumination, the lateral component $\mathbf{K_t} = (K_x, K_y)$ of the vector $\mathbf{K} = (\mathbf{K_t}, K_z)$ defines the position of the point source. Each of these imaginary point sources creates a plane wave in the object space with a different vector $\mathbf{K_t}$. Thus the contribution of all point sources creating the whole source S can be computed by integration of (1) over all lateral components $\mathbf{K_t}$. In our computations, we will not integrate the whole summation (1), but only the third term $u_o u_r^*$, which we will call a signal. This is usual in holography, as it contains the complex object amplitude. Signal from the whole source $w(\mathbf{q_t^i})$ is computed as follows:

$$w(\mathbf{q_t^i}) = \iint\limits_{(K_x^2 + K_y^2)^{1/2} < \mathrm{NA_{ill}}/\lambda} u_o(\mathbf{q_t^i}, K_x, K_y) u_r^*(\mathbf{q_t^i}, K_x, K_y) \mathrm{d}K_x \mathrm{d}K_y, \tag{2}$$

where $\mathrm{NA_{ill}} = n \sin\alpha$, n is the index of refraction in object space, α is the aperture angle of the beam entering object planes Sp and R. λ is the beam wavelength in vacuum.

2.4. The complex amplitude in the object arm

The analysis is carried out in two dimensions, x and z, as the numerical computations for three dimensional case are too demanding for a conventional computer. The lateral dimension y is dropped, however the analysis we develop is readily extended to the y dimension also.

Source, object, diffuser and output planes change into straight lines, anyway the term "planes" will be preserved for the sake of clarity. Vector $\mathbf{K}$ becomes two dimensional $\mathbf{K} = (\mathbf{K}_x, \mathbf{K}_z)$ and signal will be expressed then as follows:

#193887 - $15.00 USD Received 29 Aug 2013; revised 11 Nov 2013; accepted 17 Dec 2013; published 18 Feb 2014

$$w(x_i) \quad = \quad \int_{-\mathrm{NA_{ill}}/\lambda}^{\mathrm{NA_{ill}}/\lambda} u_o(x_i, K_x) u_r^*(x_i, K_x) \mathrm{d}K_x. \tag{3}$$

In order to express the complex amplitude of the object wave in the output plane we used the Fresnel (paraxial) approximation. Analysis could be provided non-paraxially as well, which would be more precise, but too complicated for purpose of this publication. The paraxial model gives us simple but still good insight into the studied problem. The analysis was made with the aid of the simplified drawing of the object arm in Fig. 3. The objective was approximated by thin lens L with a transmission function derived by Goodman in [31]. The numerical aperture of the objective is determined by an aperture Ap with radius R_p. The aperture is placed in the back focal plane of lens L, as we assume the objective is telecentric. Aperture Ap is not depicted in Fig. 1 since it is a part of the microscope objective. The influence of aperture is expressed by transmission function rect $\left(\frac{x_f}{2R_p}\right)$, where rect is a Rectangle function (see [31]).

A spherical wave emitted by a point source is transformed by condenser and collector lenses into plane wave having in object space a wave vector $2\pi\mathbf{K}(K_x, K_z)$. This plane wave passes through a planar object placed in the object plane Sp, having the transmission function $t_0(x_0)$. This wave is then scattered by a thin(one layer) diffuser D with transmission function $t_d(x_d)$, which is defined numerically. Then it propagates through aperture Ap into the output plane OP, where the wave is studied. The propagation between individual planes is computed with the use of the Fresnel propagators.

The output plane OP in Fig. 3 is depicted in the place of the image plane of the objective. In fact, in a CCHM there are two more optical components between objective and the output plane - output lens and tube lens. However, these two lenses can transmit all frequencies transmitted by the objective. Therefore placing the output plane into the image plane of the objective doesn't introduce any frequency loss.

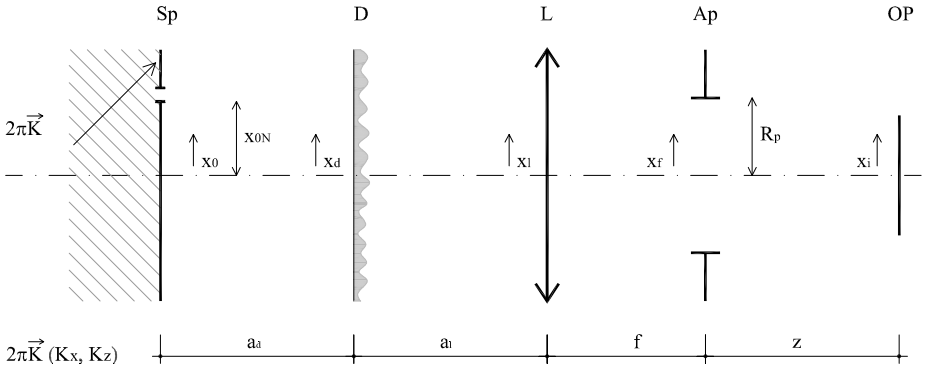

Fig. 3. Simplified drawing of the object arm for computation of the amplitude in the output plane when imaging a planar object placed in the object plane Sp. In this Fig. the object is a point aperture at coordinate $x_0 = x_{0\mathrm{N}}$. D...diffuser, L...thin lens substituting the objective, Ap...aperture diaphragm in the back focal plane of thin lens, OP...output plane.

#193887 - $15.00 USD Received 29 Aug 2013; revised 11 Nov 2013; accepted 17 Dec 2013; published 18 Feb 2014

2.5. Computation of PSF in the object arm

In this part we will demonstrate the PSF of the object arm computed according to Sec. 2.4. If an opaque screen with a point aperture is placed in the object plane Sp at coordinate $x_0 = x_{0\mathrm{N}}$ (Fig. 3), then its transmission function is $t_0(x_0) = \delta(x_0 - x_{0\mathrm{N}})$. The complex amplitude of the object wave in the output plane is then denoted by $\eta_{\mathrm{obj}}(x_i, K_x)$ and it is equal to

$$\begin{aligned} \eta_{\mathrm{obj}}(x_i, K_x) &= C\exp(i2\pi K_x x_{0\mathrm{N}})\exp\left(\frac{i\pi K x_{0\mathrm{N}}^2}{a_d}\right)\exp\left(\frac{i\pi K x_i^2}{z}\right)\times \\ &\times \int_{-\infty}^{\infty} t_d(x_d) I \exp\left[\frac{i\pi K}{a_d}(-2x_{0\mathrm{N}}x_d + x_d^2)\right]\mathrm{d}x_d, \end{aligned} \tag{4}$$

where

$$I = F\left[Ee\left(R_p - \frac{B}{2A}\right) - Ee\left(-R_p - \frac{B}{2A}\right)\right], \tag{5}$$

$A = \frac{f-a_l}{2f^2} + \frac{1}{2z}$, $B = \frac{x_d}{f} + \frac{x_i}{z}$, $C = iK^4\frac{\exp[i2\pi K(a_d+a_l+f+n\Delta_0+z)]}{a_d a_l f z}$, $F = \exp\left(-i\pi K\frac{B^2}{2A}\right)\sqrt{\frac{1}{4KA}}$, where n is the refraction index of the lens L and Δ_0 is the lens thickness measured along the optical axis.

The function $Ee(x)$ is a sum of Fresnel integrals [32]

$$Ee(x) = C(x) + iS(x) = \int_0^x \exp\left(i\frac{\pi}{2}t^2\right)\mathrm{d}t \tag{6}$$

The exact meaning of $\eta_{\mathrm{obj}}(x_i, K_x)$ is a complex amplitude in the output plane in the object arm at coordinate x_i when imaging a point aperture placed in the object plane at coordinate $x_{0\mathrm{N}}$. This point aperture is illuminated by plane wave with a wave vector $2\pi\mathbf{K} = 2\pi(K_x, K_z)$. In order to call η_{obj} PSF, both linearity and spatial invariance in η_{obj} must be fulfilled. The equation (4) shows, that imaging process described by $\eta_{\mathrm{obj}}(x_i, K_x)$ is linear, but it is not spatially invariant, because $\eta_{\mathrm{obj}}(x_i, K_x)$ doesn't depend on the difference $x_{0\mathrm{N}} - x_i$. Terms x_i, $x_{0\mathrm{N}}$ appear in the formula (4) independently. Anyway, as it will be shown by simulations later, within certain range of $x_{0\mathrm{N}}$ the η_{obj} only shifts correspondingly to the relevant $x_{0\mathrm{N}}$ while the shape of η_{obj} is preserved. For values used in experiments of this work η_{obj} can be regarded as PSF.

2.6. Computation of the CCHM PSF

PSF of the whole microscope h_{CCHM} can be computed if we replace $u_o(x_i, K_x)$ in Eq. (3) by $\eta_{\mathrm{obj}}(x_i, K_x)$ (Eq. (4)). Then the PSF of the whole microscope h_{CCHM} is expressed as

$$h_{\mathrm{CCHM}}(x_i) = \int_{-\mathrm{NA_{ill}}/\lambda}^{\mathrm{NA_{ill}}/\lambda} \eta_{\mathrm{obj}}(x_i, K_x) u_r^*(x_i, K_x)\mathrm{d}K_x, \tag{7}$$

where $u_r(x_i, K_x)$ is the complex amplitude of the reference wave.

In contrast to the amplitude of the object wave, the reference wave is independent of the object. If we do an analogy of Eq. (4) for the reference arm, it means without diffuser ($t_d = 1$) and without any object ($t_0 = 1$), we will obtain a simple formula.

#193887 - $15.00 USD Received 29 Aug 2013; revised 11 Nov 2013; accepted 17 Dec 2013; published 18 Feb 2014

$$u_r(x_i, K_x) \quad = \quad C_{\text{ref}} \exp\left(-i2\pi K_x \frac{x_i}{M}\right), \tag{8}$$

where M is an absolute value of magnification between the output plane and the object plane. C_{ref} is a complex constant. Because of convenience from now instead of x_i coordinate we will use the conjugated coordinate $x_0 = -x_i/M$. The advantage of using x_0 instead of x_i lies in the fact, that the results are related directly to the object plane which makes the results interpretation straightforward.

In order to simplify the formula (7) for h_{CCHM} we will make factorization of (4)

$$\eta_{\text{obj}}(x_0, K_x) \quad = \quad h_{\text{obj}}(x_0) \exp(i2\pi K_x x_{0\text{N}}), \tag{9}$$

where $h_{\text{obj}}(x_0)$ contains all parts of $\eta_{\text{obj}}(x_0, K_x)$ (4) which are independent of K_x. The PSF of the whole microscope can therefore be written as

$$h_{\text{CCHM}}(x_0) = h_{\text{obj}}(x_0) C_{\text{ref}} \underbrace{\int_{-\text{NA}_{\text{ill}}/\lambda}^{\text{NA}_{\text{ill}}/\lambda} \exp\left[i2\pi K_x (x_{0\text{N}} - x_0)\right] \mathrm{d}K_x}_{h_{\text{ref}}(x_0)}. \tag{10}$$

The integral in the last formula can be assigned as h_{ref} because it is equal to

$$h_{\text{ref}}(x_0) = \frac{\sin\left[\text{NA}_{\text{ill}}(x_0 - x_{0\text{N}}) 2\pi/\lambda\right]}{\text{NA}_{\text{ill}}(x_0 - x_{0\text{N}}) 2\pi/\lambda}, \tag{11}$$

which equals the amplitude of an image of a point created by an objective with numerical aperture NA_{ill}. Here it is important to mention, that h_{ref} is not PSF of the reference arm in the real sense of the word. But similar indication was used for example in publications [14, 21] and we consider it as very illustrative. If we omit the constant C_{ref}, then we can write the PSF of the whole microscope as

$$h_{\text{CCHM}}(x_0) = h_{\text{obj}}(x_0) h^*_{\text{ref}}(x_0). \tag{12}$$

The use of the complex conjugation $h^*_{\text{ref}}(x_0)$ is pointless, while $h_{\text{ref}}(x_0)$ is a real function. In the following we will therefore write only $h_{\text{ref}}(x_0)$.

If no diffuser is placed in the object arm and if NA_{ill} is equal to the objective numerical aperture $\text{NA}_{\text{ob}} = \frac{R_p}{f}$, then

$$h_{\text{CCHM}}(x_0) = |h_{\text{obj}}(x_0)|^2 = |h_{\text{ref}}(x_0)|^2. \tag{13}$$

For clarity we will call the functions $h_{\text{obj}}(x_0)$ "the object arm PSF" and $h_{\text{CCHM}}(x_0)$ "the microscope PSF".

2.7. Image shift

For imaging in CCHM by diffuse light we will use various lateral shifts between the reference and the object arm, as described above in 2.2 and in the 2. The mutual shift is performed by

#193887 - $15.00 USD Received 29 Aug 2013; revised 11 Nov 2013; accepted 17 Dec 2013; published 18 Feb 2014

shifting the microscope objective in the reference arm laterally. If we create a mutual shift of images Δx_i in the output plane, which will be denoted by conjugated Δx_0, then the microscope PSF h_{CCHM} is expressed as

$$h_{\mathrm{CCHM}}(x_0,\Delta x_0) = h_{\mathrm{obj}}(x_0)h_{\mathrm{ref}}(x_0-\Delta x_0). \tag{14}$$

2.8. Numerical computation of the object arm PSF and the microscope PSF

A thin ground glass was used in experiments as a diffuser. The transmission function of such diffuser can be described by a function $t_d(x_d) = \exp[ik\Phi(x_d)]$ (see [33,34]). $\Phi(x_d)$ is an optical path difference caused by the diffuser at x_d, where x_d is the lateral coordinate of the diffuser surface. $\Phi(x_d)$ has a Gaussian distribution with a mean value $\mu = 0$ and variance σ determining maximum range of $\Phi(x_d)$. The coordinate x_d is divided into small segments of length $0.1\,\mu$m which equals approximately 1/6 of the wavelength $\lambda = 650\,$nm used for computations. The segments of x_d are therefore sufficiently small in comparison to the resolution of the microscope. By modifying σ value the strength of the diffuser is changed. The σ values used in the model are chosen within the interval $0.00-0.84\lambda$. In all numerical computations as well as in the experiments the numerical aperture of illuminating beam $\mathrm{NA_{ill}}$ was chosen to be equal to the numerical aperture of the microscope objective $\mathrm{NA_{ob}} = 0.25$. In order to compute the "microscope PSF"as well as "the object arm PSF" the above parameters were inserted into the model of PSF derived in 2.5 section.

2.9. The results of the numerical model

The parameters of the model were adjusted in such a way that they correspond to the experiment described in part 3. The results of the model for axial point $x_{0\mathrm{N}} = 0$ are depicted in Fig. 4 where in the left column of this Fig. the absolute value of the object arm PSF $|h_{\mathrm{obj}}(x_0)|$ together with $|h_{\mathrm{ref}}(x_0)|$ or $|h_{\mathrm{ref}}(x_0-\Delta x_0)|$ are shown. In the right column there is the absolute value of microscope PSF $|h_{\mathrm{CCHM}}(x_0)| = |h_{\mathrm{obj}}(x_0)h_{\mathrm{ref}}(x_0-\Delta x_0)|$.

Figures 4(a), 4(b)-4(d), and 4(e) represent three different realizations of the diffuser. One realization corresponds to one certain function $\Phi(x_d)$ and therefore also to a certain function $h_{\mathrm{obj}}(x_0)$. Even if both σ and μ are constant, the realization can vary substantially, as σ and μ are only statistical parameters of $\Phi(x_d)$.

Figure 4(a) shows the situation without diffuser, it means that $\sigma = 0$. The numerical simulations of h_{obj} and h_{CCHM} in Fig. 4(a) are equal to their analytical expression. In all three Figs. 4(b)-4(d) there is only one realization with $\sigma = 0.42\,\lambda$. The only difference between Figs. 4(b)-4(d) is in Δx_0. Figure 4(e) belongs to a realization of a stronger diffuser with $\sigma = 0.84\,\lambda$.

Figure 4(b) shows the PSFs in ballistic light, it is with $\Delta x_0 = 0$. The ballistic light PSFs look similar to the PSFs without diffuser (Fig. 4(a)), only the signal level has decreased approximately ten times when compared to the situation without diffuser.

Figure 4(c) shows the PSFs in diffuse light with mutual shift $\Delta x_0 = 16.0\,\mu$m. In this particular representation of the diffuser with this mutual shift the main maximum of the function h_{ref} is in the position of a local maximum of h_{obj}, therefore their product (right column) has the sharp maximum here as well. The microscope PSF in Fig. 4(c) is therefore very similar to microscope PSF in Figs. 4(a) and 4(b). On the other hand shifting the reference arm slightly by only $1.0\,\mu$m to the mutual shift $\Delta x_0 = 15.0\,\mu$m causes, that the microscope PSF looks very different. This is caused by the fact, that the main maximum of the h_{ref} coincides now with a local minimum of h_{obj}.

In Fig. 4(e) there is a different realization of the diffuser, with $\sigma = 0.84\,\lambda$. Here the ballistic peak becomes approximately three times smaller in comparison to the diffuser realization with smaller $\sigma = 0.42$ (Fig. 4(b)).

#193887 - $15.00 USD Received 29 Aug 2013; revised 11 Nov 2013; accepted 17 Dec 2013; published 18 Feb 2014

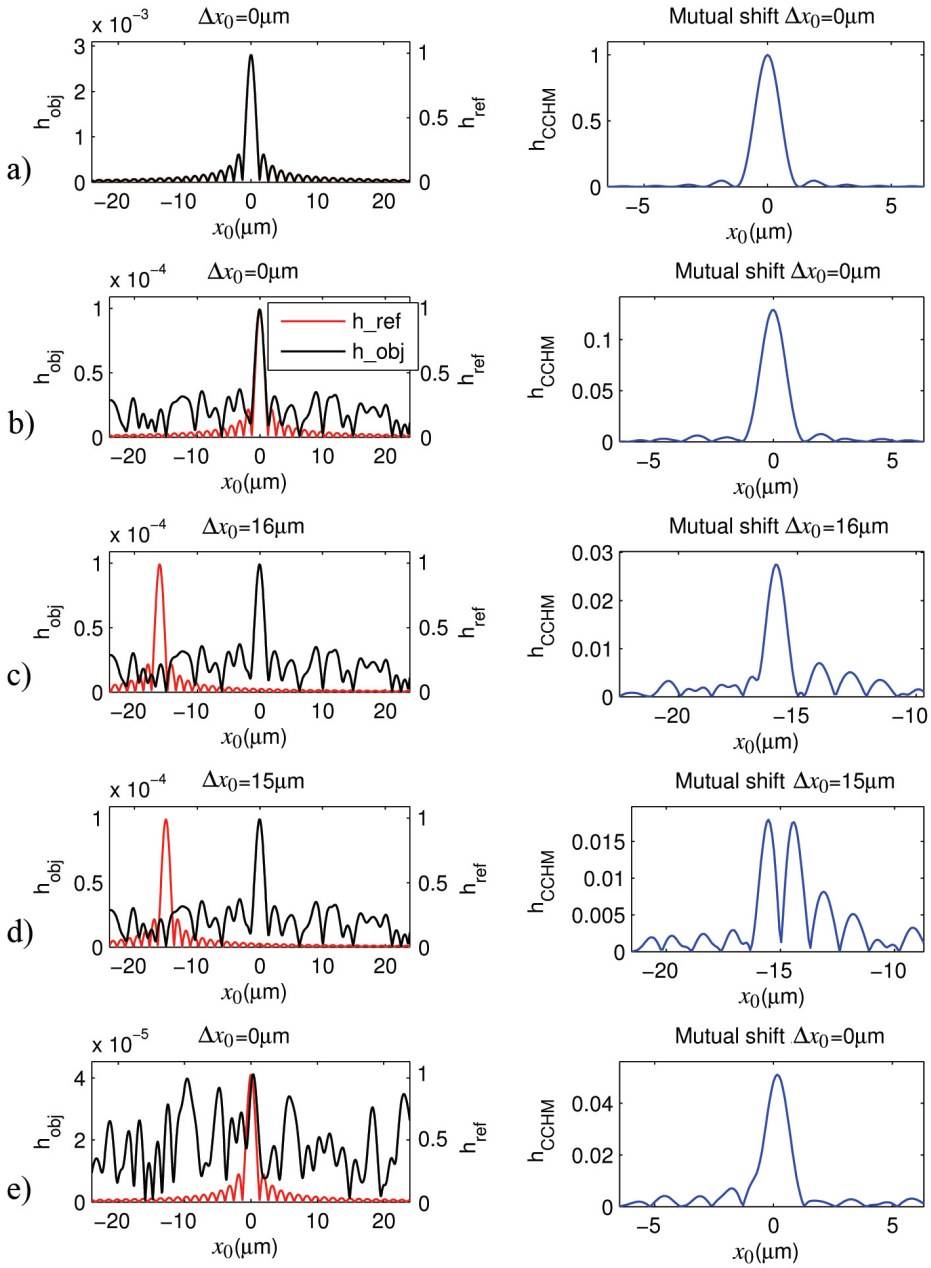

Fig. 4. In the left column there are the absolute values of function h_{obj} together with h_{ref} mutually shifted accordingly to the relevant Δx_0, in the right column there is the absolute value of their product $|h_{\mathrm{CCHM}}| = |h_{\mathrm{obj}} h_{\mathrm{ref}}|$ normalized to the maximum value of $|h_{\mathrm{CCHM}}|$ without diffuser. The row a) shows simulation without diffuser, rows b)-d) and e) respectively represent two different realizations of diffuser. Rows b)-d) represent different mutual shifts Δx_0 for the same realization of the diffuser, specifically $\sigma = 0.42\,\lambda$. In the last row e) there is the result of diffuser realization $\sigma = 0.84\,\lambda$, it means a stronger diffuser.

#193887 - $15.00 USD Received 29 Aug 2013; revised 11 Nov 2013; accepted 17 Dec 2013; published 18 Feb 2014

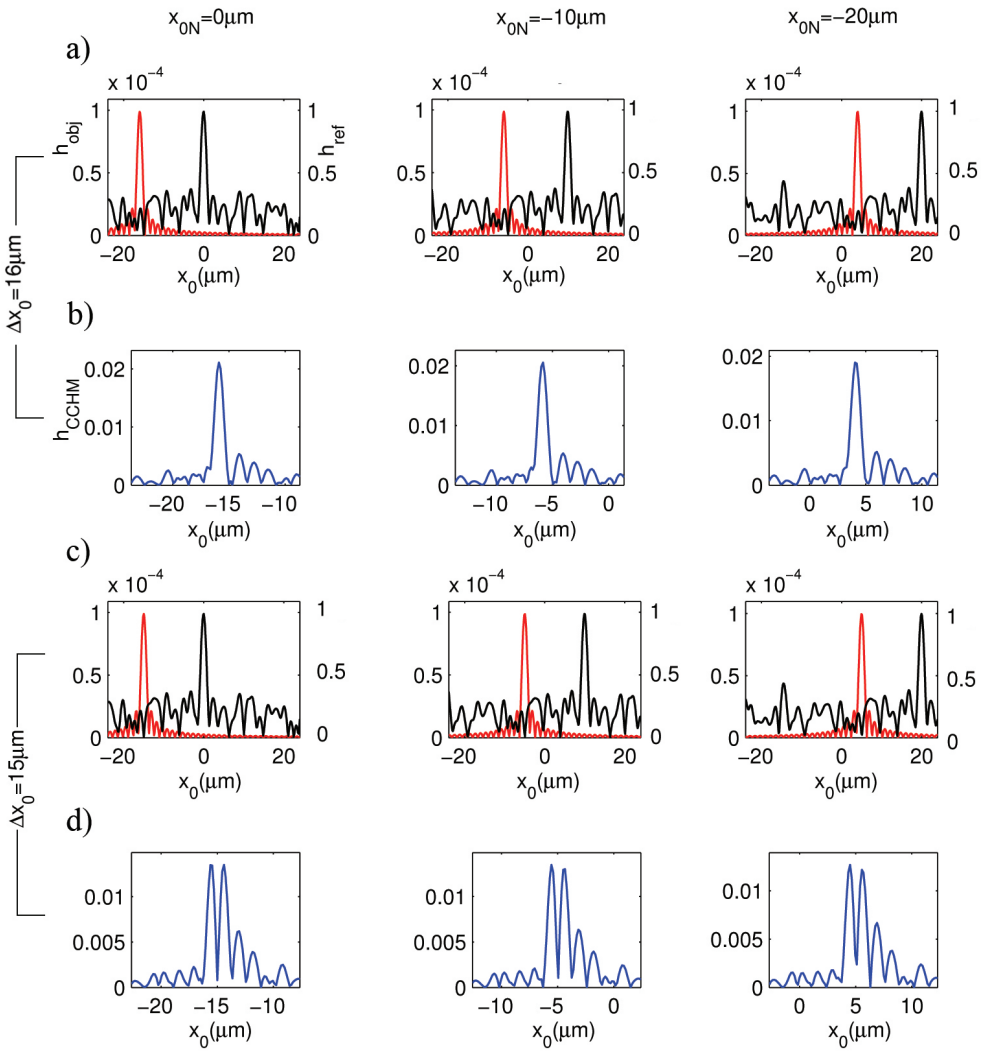

Fig. 5. Results of the PSFs for off-axis points. The first two rows a), b) represent the image with mutual shift $\Delta x_0 = 16.0\,\mu$m and following two rows c), d) $\Delta x_0 = 15.0\,\mu$m. Rows a), c) show the absolute values of functions h_{ref} (red) and h_{obj} (black) mutually shifted according to the relevant Δx_0 and rows b) and d) show the absolute value of the microscope PSF $|h_{\text{CCHM}}| = |h_{\text{obj}} h_{\text{ref}}|$. Each column shows the image for different points $x_{0\text{N}}$, consequently: axial point $x_{0\text{N}} = 0\,\mu$m and off-axis points $x_{0\text{N}} = -10\,\mu$m and $x_{0\text{N}} = -20\,\mu$m.

From the results in Fig. 4 we can conclude, that the diffuser with $\sigma = 0.42\,\lambda$ provides the best imaging properties in ballistic mode, while imaging with $\sigma = 0.84\,\lambda$ provides diffuse signal of comparable quality to ballistic signal. Anyway, in any case of the diffuser it is possible to change the microscope PSF substantially by choosing the right mutual shift Δx_0. However the right values of Δx_0 cannot be predicted by any general formula as they depend strongly on the particular realization of a diffuser. Thus also plotting or computing any dependency of image characteristics (such as RMS or resolution) on Δx_0 would not give us any general information.

The computed PSFs from Fig. 4 were used for a model of imaging a non-point object (Fig.

#193887 - $15.00 USD Received 29 Aug 2013; revised 11 Nov 2013; accepted 17 Dec 2013; published 18 Feb 2014

5). First we have to prove, whether the computed functions h_{obj} are really spatially invariant. For this purpose we have computed h_{obj} for off-axis points $x_{0\mathrm{N}} = -10\,\mu$m and $x_{0\mathrm{N}} = -20\,\mu$m for one realization of diffuser from Fig. 4(b) and we have compared it to h_{obj} for the axial point $x_{0\mathrm{N}} = 0\,\mu$m with the same realization of diffuser. All plots in Fig. 5 illustrate only one realization which is equal to realization from Figs. 4(b)-4(d). Figures 5(a) and 5(b) show the results of simulation for mutual shift $\Delta x = 16.0\,\mu$m, while in Figs. 5(c) and 5(d), the mutual shift is $\Delta x = 15.0\,\mu$m.

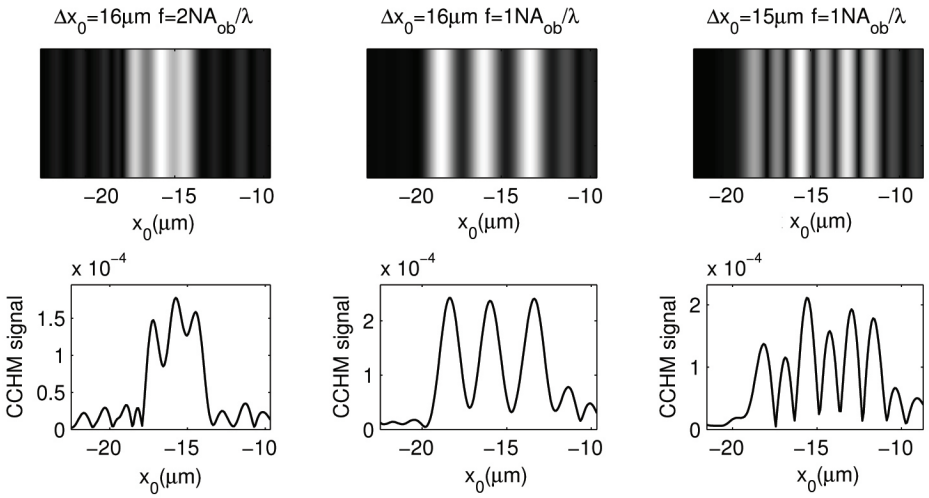

Fig. 6. Numerical simulation of imaging three infinite equidistant parallel slits. In the upper row there is a computed signal in the gray scale. In the bottom row, there is a plot profile of the upper row. In the left column the spatial frequency of slits is $f = 2\mathrm{NA}_{\mathrm{ob}}/\lambda$ and the mutual shift $\Delta x_0 = 16.0\,\mu$m, in the middle column $f = \mathrm{NA}_{\mathrm{ob}}/\lambda$, $\Delta x = 16.0\,\mu$m and in the right column $f = \mathrm{NA}_{\mathrm{ob}}/\lambda$, $\Delta x = 15.0\,\mu$m.

The first column of Fig. 5 corresponds to an axial point $x_{0\mathrm{N}} = 0\,\mu$m, the second column of Fig. 5 corresponds to an off-axis point $x_{0\mathrm{N}} = -10\,\mu$m and the third column to $x_{0\mathrm{N}} = -20\,\mu$m. Function h_{obj} (black color) with h_{ref} (red color) are depicted in Figs. 5(a)-5(c). Functions representing signal, product $h_{\mathrm{obj}}h_{\mathrm{ref}}$, are displayed in Figs. 5 (b) and 5(d) in such a way that the main maximum is plotted at the center of the horizontal axis. By changing $x_{0\mathrm{N}}$ functions $h_{\mathrm{ref}}, h_{\mathrm{obj}}$ and h_{CCHM} are only shifted in the x_0 axis according to the relevant $x_{0\mathrm{N}}$, but their shape remains unchanged. Therefore we can assume that $h_{\mathrm{obj}}, h_{\mathrm{CCHM}}$ are spatially invariant at least in the interval $x_{0\mathrm{N}} \in [-20, 20]\,\mu$m, thus within experiments of this article we can consider it as PSF.

In Fig. 6 there are simulated images of three identical and equidistant infinite transparent parallel slits. The transmission function of these slits is described by $t(x_0)$. $t(x_0) = 1$ inside the slits, and $t(x_0) = 0$ outside of slits. The images were obtained by convolution of $t(x_0)$ with the microscope PSF. The CCHM signal is then computed as

$$w(x_0) = \int_{-\infty}^{\infty} t(x_0')h_{\mathrm{CCHM}}(x_0 - x_0')\mathrm{d}x_0'. \tag{15}$$

The upper row of Fig. 6 shows the signal in a gray scale, the lower row is its plot profile. Depicted are only the results with the same realization of the diffuser as in Figs. 4(b)-4(d). In the first two columns of Fig. 6, the imaged slits have the spatial frequency $f_{\mathrm{incoh}} = 2\mathrm{NA}_{\mathrm{ob}}/\lambda$

#193887 - $15.00 USD Received 29 Aug 2013; revised 11 Nov 2013; accepted 17 Dec 2013; published 18 Feb 2014

(resolution limit for microscopy in incoherent light and also the cut-off frequency of CCHM with $\mathrm{NA_{ob}} = \mathrm{NA_{ill}}$ [27]) and $f_{\mathrm{coh}} = \mathrm{NA_{ob}}/\lambda$ (resolution limit for microscopy in coherent light), respectively, and the mutual shift is $\Delta x_0 = 16.0\,\mu$m, which corresponds to PSF in Fig. 4(c). The third column of Fig. 6 displays images of slits with spatial frequency f_{coh}, but for mutual shift $\Delta x_0 = 15.0\,\mu$m, which corresponds to PSF in Fig. 4(d). We can conclude from the Fig. 6 that with mutual shift $\Delta x_0 = 16.0\,\mu$m we can image slits with spatial frequency f_{incoh}. Whereas with the mutual shift $\Delta x_0 = 15.0\,\mu$m even two times lower frequency f_{coh} is not resolved.

3. Experimental results

The experiment was carried out on CCHM. The optical setup of the microscope is shown in Fig. 1. We have used objectives Nikon $10\times/0.25$. The light source was a halogen lamp. The aperture angle of the illuminating beam was chosen to fill the aperture of the microscope objectives completely ($\mathrm{NA_{ill}} = \mathrm{NA_{ob}}$). In order to obtain the quasi-monochromatic light, the interference filter was used ($\lambda_0 = 650\,$nm FWHM $10\,$nm). This implies the coherence length (CL) approximately $42\,\mu$m. Thanks to the large coherence length together with very narrow bandwidth the effect of dispersion caused by specimen or diffuser is negligible. The fact that we use quasi-monochromatic light (the large coherence length) also explains why the longitudinal shifts in reference arm were not performed.

We used a resolution chart as a specimen and a thin ground glass of thickness $0.17\,$mm as a diffuser. The distance between the diffuser and the specimen was $a_d = 4\,$mm.

Compare now the results of simulation of the line objects image with the results of the experiment. Figure 7 shows the measured signal w in a gray scale. The original holograms, especially those made through diffuser, are not presented here with respect to their very low contrast. In the first column of Fig. 7 there is an image of the resolution chart which is displayed in detail in the second and the third column of Fig. 7. Figure 7(a) shows an image without diffuser and the Figs. 7(b)-7(e) show images made with diffuser. The only difference between images made with diffuser was in the mutual shift Δx_0 implemented by lateral shift of the objective in the interferometer. The variance of $t_d(x_d)$ of the experimental diffuser can be estimated to be similar to a model diffuser from Figs. 4(b)-4(d). Ballistic image $\Delta x_0 = 0$ is in Fig. 7(b), while diffuse light images are in Figs. 7(c)-7(e). The mutual shifts are consequently $\Delta x_0 = 44,8\,\mu$m - Fig. 7(c), $\Delta x_0 = 42.7\,\mu$m - Fig. 7(d) and $\Delta x_0 = 47.0\,\mu$m - Fig. 7(e). In each of these images the resolution is different and it is illustrated by the orange label around lines with a spatial frequency on the resolution limit. In Fig. 7(a) the resolution is $f_{\mathrm{lim}} = 0.81 f_{\mathrm{incoh}}$, in ballistic light image, Fig. 7(b), $f_{\mathrm{lim}} = 0.73 f_{\mathrm{incoh}}$. Theoretically it should be possible to image lines having frequency $f_{\mathrm{lim}} = f_{\mathrm{incoh}}$, but experimentally this limit was not achieved. It has more reasons, first is that CTF has very low value for frequencies near to f_{incoh}, the other reason rests in the fact that the image suffers from aberrations, mainly spherical. Lower resolution of ballistic image is moreover influenced also by the lower SNR level.

The limit frequencies measured for diffuse light in CCHM are $f_{\mathrm{lim}} = 0.73 f_{\mathrm{incoh}}$ for $\Delta x_0 = 44.8\,\mu$m, $f_{\mathrm{lim}} = 0.48 f_{\mathrm{incoh}}$ for $\Delta x_0 = 42.7\,\mu$m and $f_{\mathrm{lim}} = 0.53 f_{\mathrm{incoh}}$ for $\Delta x_0 = 47.0\,\mu$m.

In order to obtain higher resolution images some attempts of averaging images from various mutual shifts Δx_0 were performed. But it didn't prove any significant results so far. At the moment we are trying to develop a new method for averaging from various Δx_0.

4. Conclusions

The main aim of this publication was to show the principle and some basic properties of coherence gating of diffuse light in LCI. Therefore the simple model of PSF for imaging through thin diffuse medium by CCHM was established on the basis of the 2-D model of CCHM in Fresnel (paraxial) approximation. Although CCHM is achromatic we limited the computations as well

#193887 - $15.00 USD Received 29 Aug 2013; revised 11 Nov 2013; accepted 17 Dec 2013; published 18 Feb 2014

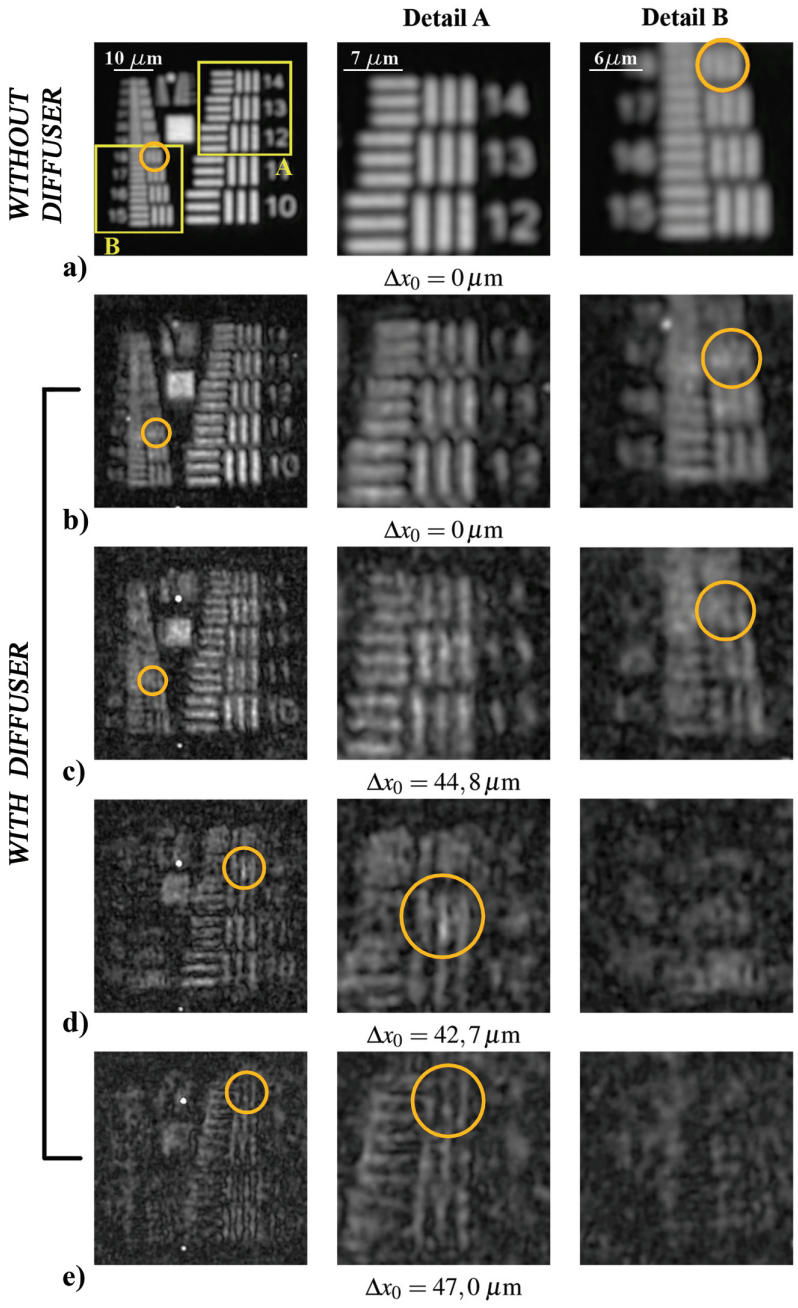

Fig. 7. The experimental results of imaging a resolution chart. The images were performed with objectives $10\times/0.25$. Interference filter $\lambda = 650\,\text{nm}$, 10 nm FWHM. a) imaging without diffuser, b) imaging with diffuser - ballistic light, c)-e) imaging with diffuser - diffuse light. The mutual shifts are c) $\Delta x = 44.8\,\mu\text{m}$ d) $\Delta x = 42.7\,\mu\text{m}$, e) $\Delta x = 47.0\,\mu\text{m}$. In the second and third column there are magnified details A and B respectively. Orange circles indicate the resolution limit of images in the corresponding row.

#193887 - $15.00 USD Received 29 Aug 2013; revised 11 Nov 2013; accepted 17 Dec 2013; published 18 Feb 2014

as the experiments only for monochromatic light. By doing this the experimental results can be interpreted and compared with computations more easily.

The equation for PSF was derived analytically, nevertheless in order to obtain a quantitative solution we had to use numerical computation, since the diffuser transmission function is generated as a random function with a mesh fine enough when compared to the resolution of the microscope. The results of numerical computation were compared with the analytical expressions for CCHM without diffuser.

A significant peak was obtained as a result of simulation of PSF for imaging through weakly scattering diffuser in ballistic light. At the same time we show, that the image can be obtained in diffuse light as well. The diffuse light PSF depends on the parameter Δx_0, which denotes the mutual lateral shift between the reference and the object arms in the output plane. Choosing a right value of Δx_0 leads to PSF similar to the situation without diffuser. On the other hand even the small change of Δx_0 from the right value can deform the PSF very significantly.

The influence of a stronger diffuser on the microscope PSF was studied as well. The ballistic peak becomes not as significant as in the case of a weaker diffuser. However, for the diffuse light imaging, the findings for PSF remain unchanged.

In the experiment we have proved the computed results for a weaker diffuser by imaging a resolution chart through a ground glass. We have also shown experimentally the strong influence of the mutual shift Δx_0 on the microscope PSF. In diffuse light by choosing a right value of Δx_0 we were able to image objects with spatial frequency near to the theoretical resolution limit for CCHM without diffuser $2\mathrm{NA}/\lambda$. However, this theoretical limit is not fully achieved mainly due to the low SNR level. When the Δx_0 was changed from this right value, the PSF changed rapidly which resulted in an image of much lower quality and resolution. This is in accordance with the results of the model. However the particular values of Δx_0 are not the same for the experimental and for the model results. This is caused by the fact that the model diffuser is defined by the transmission function, which is generated numerically as a matrix of random phase shifts and thus it can hardly be equal to the transmission function of a real diffuser.

Acknowledgments

The authors thank to colleagues from Experimental biophotonics group (CEITEC) for helpful discussions, especially to Věra Kollárová, Pavel Kolman, Matěj Týč, Jiří Komrska, and Zbyněk Dostál. This work was supported by Technology Agency of the Czech Republic (TE01020229), Ministry of Industry and Trade of the Czech Republic (FR-TI4/660), CEITEC – Central European Institute of Technology (CZ.1.05/1.1.00/02.0068) from European Regional Development Fund and by the grant "Specific research" FSI-S-11-22 of Brno University of Technology.

#193887 - $15.00 USD Received 29 Aug 2013; revised 11 Nov 2013; accepted 17 Dec 2013; published 18 Feb 2014